ORGANOMETALLICS

Article

pubs.acs.org/Organometallics

Synthesis, Characterization, and Infrared Reflectance Spectroelectrochemistry of Organoruthenium Nitrosyl Porphyrins

Nan Xu,* John Lilly, Douglas R. Powell, and George B. Richter-Addo*

Department of Chemistry and Biochemistry, University of Oklahoma, 101 Stephenson Parkway, Norman, Oklahoma 73019, United States

Supporting Information

ABSTRACT: Metal−carbon bonds are known to form during the metal-catalyzed transformations of various organic compounds such as phenylhydrazines by the heme-containing proteins cytochrome P450, hemoglobin, and myoglobin. The preparation and characterization of synthetic organometallic porphyrins of the group 8 metals are thus of interest, and their properties help enlighten the general discussion of metalloporphyrin−carbon bond chemistry. We have prepared a representative set of (por)Ru(NO)R compounds (por = T(*p*-OMe)PP, T(*p*-CF_3)PP; R = Me, Et) containing Ru−alkyl bonds trans to NO. We have determined the X-ray crystal structure of (T(*p*-OMe)PP)Ru(NO)Et, which represents the first crystal structure reported for any organometallic nitrosyl porphyrin with an alkyl ligand trans to NO; the structure reveals a significantly bent RuNO moiety at 153° in this {RuNO}^{6} compound. We have characterized the redox behavior of the (T(*p*-OMe)PP)Ru(NO)-containing compounds by cyclic voltammetry and infrared spectroelectrochemistry, and we have determined that the first oxidations are porphyrin-centered.

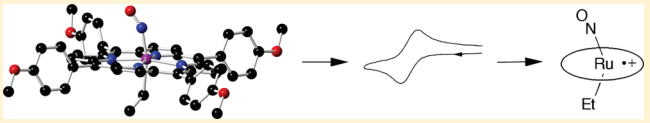

INTRODUCTION

Metal−carbon bonds form during the reactions of some substrates with the heme proteins myoglobin (Mb), hemoglobin (Hb), and cytochrome P450.[1−4] For example, σ-bonded aryliron(III) complexes form when phenylhydrazines (e.g., $PhNHNH_2$) react with Hb[5] and Mb.[6] The occurrence of metal−carbon bonds in biology has spurred an interest in the preparation and study of metalloporphyrin model systems of the group 8 metals, including their redox behavior.

A number of organometallic heme models of the group 8 metals have been synthesized and characterized.[7−23] They can generally be prepared via one or more synthetic routes: (i) reaction of a precursor (por)metal halide (por = porphyrinato dianion) with an alkylating agent (R−M; M = main-group metal; R = alkyl, aryl),[17,19] (ii) reaction of a metalloporphyrin anion with an alkyl halide,[24] and (iii) reaction of a metalloporphyrin cation with an alkylating agent (R−M).[25] Both five- and six-coordinate organometallic porphyrins have been reported. The redox behavior of several of these compounds has been studied by electrochemistry,[26] although studies on the redox behavior of organoruthenium porphyrins have lagged behind those of other organometallic porphyrins. Seyler and Leidner reported the cyclic voltammetric behavior of (OEP)$Ru(Ph)_2$ and demonstrated a Ru-to-N_{por} migration of an initially Ru-bound Ph group upon oxidation (the identity of the product was confirmed by X-ray crystallography).[17] They found that an alkyl migration from Ru to N_{por} also occurred when (OEP)$RuMe_2$ was chemically oxidized to give the $[$(OEP-*N*-Me)RuMe$]^+$ derivative.[18] In contrast, the non-organometallic complexes (por)Ru(NO)X (X = halide,[27] pseudohalide,[28−30] $[H_2O]^+$[30,31]) undergo electrochemical oxidations that do not involve migration of the axial non-nitrosyl ligand to a porphyrin N atom.

Some organometallic (por)M(NO)R compounds have been reported for Fe,[7,10,12,32] Ru,[32,33] and Os.[34] Crystal structure data for (OEP)Fe(NO)(C_6H_4F-*p*),[32] (OEP)Ru(NO)(C_6H_4F-*p*),[32] and (TTP)Ru(NO)(C_6H_4F-*p*)[33] revealed a cisoid bending of the axial NO and aryl ligands from the heme normal. Results from theoretical calculations on these structurally characterized aryl compounds have helped explain the inherent stabilization of the cisoid structures (i.e., deviation from standard octahedral geometry).[32,35] No (por)M(NO)(*alkyl*) derivative has been structurally characterized by X-ray diffraction, however. Thus, we were uncertain whether the axial ligand bending and resulting stabilization will be applicable to the alkyl systems as well.

There have been only a handful of electrochemical studies on organoruthenium porphyrins reported,[16−18] and there is no report describing the electrochemical behavior of the organometallic nitrosyl compounds (por)Ru(NO)R (R = alkyl, aryl). In this article, we report the synthesis and characterization of the (por)Ru(NO)R (R = Me, Et; por = T(*p*-OMe)PP, T(*p*-CF_3)PP) compounds, the X-ray crystal structure of the (T(*p*-OMe)PP)Ru(NO)Et derivative, the redox behavior of the compounds at a Pt-disk electrode, and the IR spectroelectrochemical results that help establish the identities of the redox products.

Received: July 7, 2011
Published: January 17, 2012

RESULTS AND DISCUSSION

Synthesis and Characterization. Prior to this work, only three organoruthenium nitrosyl porphyrins had been reported, namely the alkyl compound (TTP)Ru(NO)Me[33] and the aryl compounds (TTP)Ru(NO)(C_6H_4F-*p*)[33] and (OEP)Ru(NO)-(C_6H_4F-*p*).[32] Reactions of the precursor (T(*p*-X)PP)Ru(NO)-Cl[27] compounds with AlR_3 or RMgBr (R = Me, Et) reagents resulted, after appropriate workup, in the generation of the target (T(*p*-X)PP)Ru(NO)R (R = Me, Et) derivatives in moderate to low isolated yields. We found that laboratory lighting decomposed these organometallic products (e.g., ~10% decomposition over 10 h, as judged by NMR spectroscopy); hence, we utilized reduced laboratory lighting in our preparations and purifications.

When the Grignard reagent MeMgBr is used in place of $AlMe_3$ in the alkylation reaction, the (T(*p*-OMe)PP)Ru(NO)-Me product is generated in a lower isolated yield. A similar lower isolated yield for (T(*p*-OMe)PP)Ru(NO)Et was obtained using EtMgBr. In general, we find that large excesses of the Grignard reagents and longer reaction times result in lower yields of the desired products (not shown), presumably due to follow-up reactions of the (T(*p*-OMe)PP)Ru(NO)R products with excess reagents to yield the *trans*-dialkyl products. Such reactions with excess Grignard reagents have been reported previously by us for the reaction of (TTP)Ru-(NO)Cl with MeMgBr; the target (TTP)Ru(NO)Me and the dialkyl (TTP)Ru$(Me)_2$ byproduct proved very difficult to separate, due to their similar solubilities in organic solvents.[33]

IR and ^{1}H NMR Spectroscopy. IR nitrosyl stretching frequencies of the organoruthenium nitrosyl complexes reported to date and selected chloro precursors are given in Table 1. The ν_{NO}s of the (por)Ru(NO)R compounds are much lower than those of their chloro precursors. For example, the ν_{NO} for (T(*p*-CF_3)PP)Ru(NO)Me as a KBr pellet is at 1735 cm^{-1}, which is 112 cm^{-1} lower than that of (T(*p*-CF_3)PP)Ru-(NO)Cl at 1847 cm^{-1}, and this reflects the strong σ donor property of the methyl ligand. In addition, although there is no clear trend with the ν_{NO} values of the Me vs the Et compounds as KBr pellets, it is evident from the data that the (T(*p*-X)PP)Ru(NO)Me compounds in CH_2Cl_2 have higher ν_{NO}s than the (T(*p*-X)PP)Ru(NO)Et analogues. We also note that the ν_{NO} of the previously reported aryl compound (TTP)Ru-(NO)(C_6H_4F-*p*) at 1773 cm^{-1} is 30 cm^{-1} higher than that of its alkyl derivative (TTP)Ru(NO)Me, which is consistent with the better overall electron donating ability of alkyl groups compared to aryl groups. In any event, the presence of strongly σ donating alkyl groups trans to NO results in low ν_{NO}s for this class of (T(*p*-X)PP)Ru(NO)R compounds.

Table 1. IR Nitrosyl Stretching Frequencies of Organoruthenium Nitrosyl Porphyrins and Their Precursors

compd	ν_{NO} (KBr, cm^{-1})	ν_{NO} (CH_2Cl_2, cm^{-1})	ref
(T(*p*-OMe)PP)Ru(NO)Cl	1844	1851	27
(T(*p*-CF_3)PP)Ru(NO)Cl	1847	1855	27
(OEP)Ru(NO)Cl	1829	1842	27
(T(*p*-OMe)PP)Ru(NO)Me	1735	1742	this work
(T(*p*-OMe)PP)Ru(NO)Et	1724	1723	this work
(T(*p*-CF_3)PP)Ru(NO)Me	1735	1748	this work
(T(*p*-CF_3)PP)Ru(NO)Et	1735	1735	this work
(TTP)Ru(NO)Me	1743		33
(TTP)Ru(NO)(C_6H_4F-*p*)	1773		33
(OEP)Ru(NO)(C_6H_4F-*p*)	1759		32

The ^{1}H NMR spectra of the (T(*p*-X)PP)Ru(NO)R compounds reveal upfield signals due to the alkyl ligands (Table 2). The methyl ^{1}H signals in both (T(*p*-X)PP)Ru-(NO)Me compounds described in this work, and that of (TTP)Ru(NO)Me,[33] appear as singlets at −6.7 ppm in $CDCl_3$. This large upfield shift of the $-CH_3$ signals is due to the presence of the NO ligand and the deshielding effect of the porphyrin macrocycle: cf. the $-CH_3$ signals of the dialkyl compounds (T(*p*-CF_3)PP)Ru$(Me)_2$ (−2.71 ppm), (TTP)Ru-$(Me)_2$ (−2.74 ppm in $CDCl_3$),[25,33] (OEP)Ru$(Me)_2$ (−3.51 ppm in THF-d_8)[25] and the alkyl/aryl compound (OEP)Ru-(Ph)Me (−2.74 ppm in C_6D_6).[25] The axial ethyl Ru−CH_2CH_3 ^{1}H resonances in the (T(*p*-X)PP)Ru(NO)Et compounds reveal an interesting feature attributed to the presence of the trans NO ligand. The axial methylene $-CH_2CH_3$ resonances in the (T(*p*-X)PP)Ru(NO)Et compounds are ~1.8 ppm upfield from those of the $-CH_2CH_3$ methyl resonances (Table 2). However, the reverse trend holds for the non-nitrosyl diethyl compound (T(*p*-CF_3)PP)Ru$(CH_2CH_3)_2$ (CH_2 at −1.90 ppm and CH_3 at −4.04 ppm; this work) and the previously reported diethyl compounds (OEP)Ru$(CH_2CH_3)_2$ (CH_2 at −2.74 ppm and CH_3 at −4.54),[23] (TTP)Ru$(CH_2CH_3)_2$ (CH_2 at −1.97 ppm and CH_3 at −4.08 ppm).[24]

Table 2. ^{1}H NMR Spectral Data (in ppm) for the Axial Alkyl Ligands in (por)Ru(NO)R and (por)Ru$(R)_2$ Complexes in $CDCl_3$

compd	δ(Ru−CH_3)	δ(Ru−CH_2CH_3)	δ(Ru−CH_2CH_3)
(T(*p*-OMe)PP)Ru(NO)Me	−6.72 (s)		
(T(*p*-OMe)PP)Ru(NO)Et		−6.00 (q)	−4.19 (t)
(T(*p*-CF_3)PP)Ru(NO)Me	−6.71 (s)		
(T(*p*-CF_3)PP)Ru(NO)Et		−5.96 (q)	−4.17 (t)
(T(*p*-CF_3)PP)Ru$(Me)_2$	−2.71 (s)		
(T(*p*-CF_3)PP)Ru$(Et)_2$[a]		−1.90 (q)	−4.04 (t)

[a]Identified by ^{1}NMR spectroscopy as a minor product during the preparation of the nitrosyl compound (T(*p*-CF_3)PP)Ru(NO)Et.

Crystal Structure of (T(*p*-OMe)PP)Ru(NO)Et. We reported the X-ray crystal structures of the aryl compounds (por)Ru(NO)(C_6H_4F-*p*) (por = TTP, OEP).[32,33] It proved nontrivial to obtain a suitable crystal of any *alkyl* derivative for an X-ray diffraction study, due presumably to their light sensitivity and high reactivity of nitrosyl alkyl derivatives with trace acid in halogenated solvents, in which they were soluble. We were finally able, after a multiyear effort, to obtain a suitable crystal of (T(*p*-OMe)PP)Ru(NO)Et for an X-ray diffraction study from the slow anaerobic evaporation (in the dark) of a CH_2Cl_2/hexane (2/1) solution of the complex in the presence of a trace amount of benzene.

The molecular structure of (T(*p*-OMe)PP)Ru(NO)Et is shown in Figure 1a. The axial NO and ethyl ligands are disordered across the porphyrin plane, and the disordered components were best modeled in a 55/45 ratio. The relative positions of the axial ligands with respect to the porphyrin plane of the major disordered component are shown in Figure

dx.doi.org/10.1021/om200601g | *Organometallics* 2012, 31, 827−834

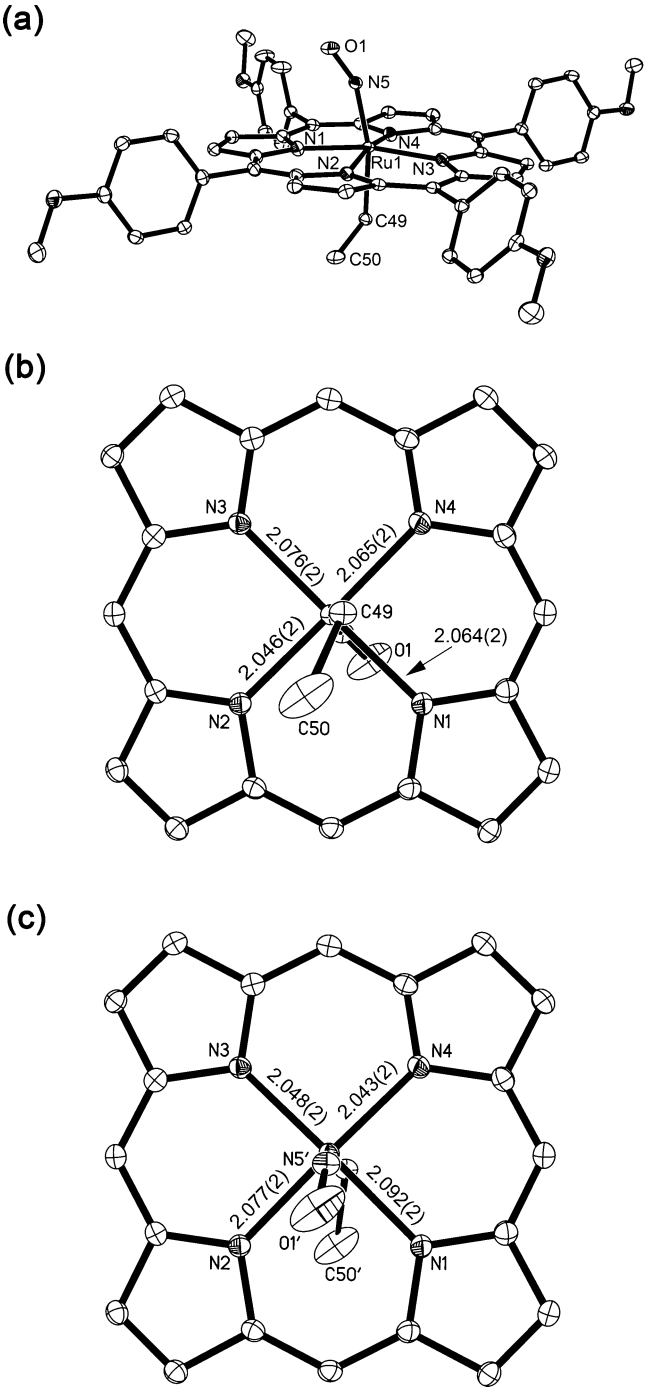

Figure 1. (a) Molecular structure of (T(*p*-OMe)PP)Ru(NO)Et. Hydrogen atoms have been omitted for clarity. Only one of the two disordered components is shown. (b) View of the porphyrin core showing the major disordered component of the axial ligands, with the ethyl group facing the viewer. (c) View of the porphyrin core showing the minor disordered component of the axial ligands, with the NO group facing the viewer.

1b, and those of the second component are shown in Figure 1c. Selected bond lengths and angles are given in Table 3.

The porphyrin core is saddled, and the Ru−N_{por} bond lengths in (T(*p*-OMe)PP)Ru(NO)Et are in the 2.043(2)−2.092(2) Å range. The Ru atom is displaced by 0.18 Å (major component) and 0.23 Å (minor component) from the 24-atom mean porphyrin plane toward the nitrosyl ligand. To the best of our knowledge, this is the first reported crystal structure of a nitrosyl alkyl porphyrin for any metal.

Table 3. Selected Bond Lengths (Å) and Angles (deg) for (T(*p*-OMe)PP)Ru(NO)Et[a,b]

N5−O1	1.139(6) [1.145(7)]	O1−N5−Ru1	153.4(5) [153(1)]
Ru1−N5	1.825(5) [1.827(5)]	N5−Ru1−C49	165.1(3) [166.8(3)]
Ru1−C49	2.117(7) [2.116(7)]	Ru1−C49−C50	118.9(7) [122.2(9)]
C49−C50	1.525(9) [1.523(10)]		

[a]Data for the second component of the disordered axial groups are given in brackets. [b]The Ru atom is apically displaced by 0.18 Å [0.23 Å] from the 24-atom porphyrin plane toward the NO ligand.

The Ru−N−O angle in this formally {RuNO}^{6} compound is bent with an angle of 153.4(5)° for the major component (153(1)° for the minor disordered component). Such a bending of metal−NO bonds in {MNO}^{6} compounds has been noted previously for (TTP)Ru(NO)(C_6H_4F-*p*) (∠RuNO = 152°),[33] (OEP)Ru(NO)(C_6H_4F-*p*), (∠RuNO = 154.9(3)°),[32] and (OEP)Fe(NO)(C_6H_4F-*p*) (∠FeNO = 157.4(2)°).[32]

We determined from theoretical calculations that the nitrosyl bending in these {MNO}^{6} compounds was intrinsic and was made energetically favorable by an associated tilting of the nitrosyl N atoms from the porphyrin normal,[32] similar to that determined computationally by Ghosh and Bocian for carbonyl hemes.[36] Indeed, Ghosh has determined, from DFT calculations for the model (porphine)Fe(NO)(Ph) compound, that the metal d_{z^2} orbital is "tied up" in a bonding interaction with the axial Ph group and that the metal d_{xz} orbital is engaged in a favorable three-center bent π bond with the NO π^* orbital.[35]

The nitrosyl N atom of (T(*p*-OMe)PP)Ru(NO)Et is tilted from the normal to the porphyrin 24-atom plane by 11.9° (major) and 8.9° (minor) (α; Table 4). The NO group is further tilted by 27°, for both disordered components, from the Ru−N(O) vector in the direction away from the porphyrin normal (β; Table 4). The axial ethyl C49 atom is also tilted in the general direction of the NO tilt (γ; Table 4). This results in nonlinear axial C−Ru−N moieties displaying angles of ∼166°. Data for the related axial ligand tilting in the (por)M(NO)R compounds reported to date are collected in Table 4.

We note that most of the six-coordinate {MNO}^{6} compounds that have been structurally characterized by single-crystal X-ray diffraction (e.g., (OEP)Ru(NO)Cl[27]) display linear M−N−O geometries with no significant axial nitrosyl N atom tilting.[13,37] However, the axial ligand tilting observed in the (por)Ru(NO)R class of compounds is not limited to six-coordinate nitrosyl compounds; such tilting has been reported for some five-coordinate and six-coordinate compounds such as (OEP)Ru(Np) (12.7°; Np = neopentyl), and (TPP)Os($CH_2Si(CH_3)_3$)$_2$ (18.5, 21.8°).[38] Such tilting in the latter class of diamagnetic d^4 compounds has been attributed, on the basis of the results of DFT calculations, to the strong trans influence of the alkyl ligands that destabilize a linear axial structure.[39,40]

The Ru−N(O) bond length in (T(*p*-OMe)PP)Ru(NO)Et is 1.825(5) Å (cf. 1.827(5) Å for the minor component), and is longer than that for the related (OEP)Ru(NO)(C_6H_4F-*p*) at 1.807(3) Å which was described as being very long for a (por)Ru−NO bond. Clearly, the presence of the strong σ-donor alkyl group trans to NO is responsible for this lengthening. The Ru−C(ethyl) bond length is also long at 2.117(7) Å [2.116(7) Å], which is at the upper end of the Ru−C(sp^3-alkyl) (2.05−2.12 Å) and Ru−C(sp^2-aryl) (2.00−2.11 Å)

dx.doi.org/10.1021/om200601g | *Organometallics* 2012, 31, 827−834

Table 4. Axial Ligand Tilts (deg) in Six-Coordinate Organometallic Nitrosyl Porphyrins (por)M(NO)R

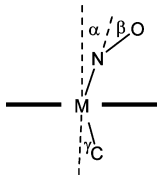

compd	α^a	β	γ^a	ref
(T(*p*-OMe)PP)Ru(NO)Et	11.9 [8.9]	27.0 [27.0]	4.8 [5.9]	this work
(TTP)Ru(NO)(C_6H_4F-*p*)	12.0	27.8	4.3	27
(OEP)Ru(NO)(C_6H_4F-*p*)	10.8	25.1	3.5	28
(OEP)Fe(NO)(C_6H_4F-*p*)	9.2	22.6	3.1	28

[a]Tilts of the N and C atoms from the normal to the porphyrin 24-atom plane.

bond length ranges for porphyrin complexes (Table 5). In comparison, the Ru−C(sp^2-carbene) bond lengths are significantly shorter, as shown in Table 5.

Table 5. Ru−C Bond Lengths in Organoruthenium (Non-Carbonyl) Porphyrin Compounds

compd	Ru−C (Å)	ref
Aryl		
(OEP)Ru(C_6H_5)	2.005(7)	21
(OEP)Ru($Ph)_2$	2.093(2), 2.098(2)	41
[(OEP-*N*-Ph)Ru(C_6H_5)]BF_4	1.999(4)	14
(TMP)Ru($Ph)_2$	2.076(9), 2.062(8)	42
(TTP)Ru(NO)(C_6H_4F-*p*)	2.095(6)	33
(OEP)Ru(NO)(C_6H_4F-*p*)	2.111(3)	32
Alkyl		
(OEP)Ru(Np)	2.069(7), 2.12(1)	19
(OEP)Ru($CH_2C(Me)_2Ph$)	2.053(4)	42
[(OEP)Ru(Np)]$_2$(μ-Li)$_2$	2.100(3)	19
(T(*p*-OMe)PP)Ru(NO)Et	2.117(7), 2.116(7)	this work
Carbene		
[(TTP)Ru(=CPh_2)(CH_3OH)]	1.845(3)	43
[(TTP)Ru[=C(3-$C_6H_4CF_3)_2$](py)	1.868(3)	44
[(TTP)Ru[=C($COPh)_2$](py)	1.877(8)	44
(TPP)Ru[=C($CO_2Et)_2$](MeOH)	1.829(9)	45

Finally, we note that the axial RuNO and RuEt orientations impart bond asymmetry to the equatorial Ru−N_4(por) core, as shown in Figure 1b,c. The asymmetry of the Ru−N_4(por) core for the minor component (Figure 1c) reproduces the asymmetry of the porphyrin core in (OEP)Fe(NO)(C_6H_4F-*p*);[32] namely, the Ru−N_{por} distances in the direction of the RuNO tilt are significantly longer than the Ru−N_{por} distances that are directed away from the RuNO tilt. Such a clear asymmetry was not, however, observed for the major disordered component.

Cyclic Voltammetry and Infrared Spectroelectrochemistry. No electrochemical properties of any organoruthenium nitrosyl porphyrins have been reported previously. The redox behavior of (T(*p*-OMe)PP)Ru(NO)Me and (T(*p*-OMe)PP)Ru(NO)Et in CH_2Cl_2 was examined by cyclic voltammetry. These compounds are more soluble, and exhibited greater thermal stability, than their (T(*p*-CF_3)PP)-Ru-containing analogues. The cyclic voltammograms of (T(*p*-OMe)PP)Ru(NO)Me are shown in Figure 2. The (T(*p*-OMe)PP)Ru(NO)Me compound undergoes two reversible oxidations at $E_1^{\circ\prime}$ = +0.77 V and $E_2^{\circ\prime}$ = +1.30 V vs Ag/AgCl, to generate the monocation [(T(*p*-OMe)PP)Ru(NO)Me]$^+$ and

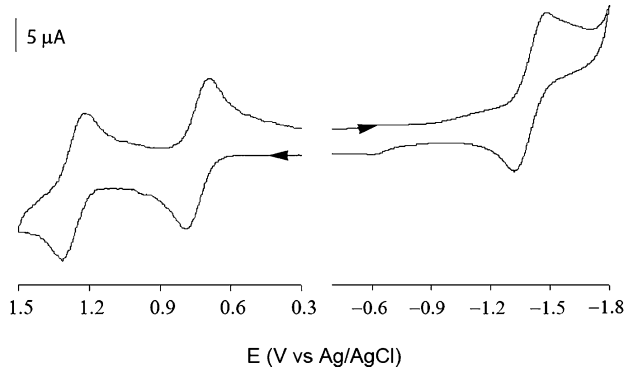

Figure 2. Cyclic voltammograms of 1 mM (T(*p*-OMe)PP)Ru(NO)-Me in CH_2Cl_2 containing 0.1 M NBu_4PF_6 at a scan rate of 0.2 V/s at room temperature. Potentials are referenced to the Ag/AgCl couple.

dication [(T(*p*-OMe)PP)Ru(NO)Me]$^{2+}$, respectively (site of oxidation not indicated; see later). In addition, these two oxidations are chemically reversible with cathodic-to-anodic peak current ratios (i_{pc}/i_{pa}) of ~1.0. Furthermore, plots of i_{pa} vs (scan rate)$^{1/2}$ for both the first and second oxidations show linear relationships, indicating that these two oxidations are diffusion-controlled. The (T(*p*-OMe)PP)Ru(NO)Me compound undergoes an electrochemically reversible reduction at −1.40 V at a scan rate of 0.2 V/s with a small daughter peak at −0.60 V. The redox couple at −1.40 V becomes less chemically reversible at lower scan rates, indicating that a slow structural change occurs (e.g., ligand loss) upon reduction.

The cyclic voltammogram of (T(*p*-OMe)PP)Ru(NO)Et (Figure 3) is more complicated than that of (T(*p*-OMe)PP)-Ru(NO)Me. When the potential scan was reversed just after the first oxidation, a well-defined reversible first redox couple ($E_1^{\circ\prime}$) was observed centered at +0.74 V (Figure 3a; i_{pc}/i_{pa} = 1), indicating chemical reversibility for this first oxidation.

A full cyclic voltammogram, however, reveals what appears to be a partially reversible first oxidation couple at +0.74 V, a second apparently irreversible process at ~+1.25 V, and a third oxidation process that approaches the solvent system limit (Figure 3b). The lower chemical reversibility of the first oxidation in the full scan is likely due to the reaction of the unstable second oxidation product with the analyte or the solvent system.

The (T(*p*-OMe)PP)Ru(NO)Et compound undergoes a reversible reduction centered at −1.47 V with a small return peak at −0.68 V. The first oxidation potentials of the (T(*p*-OMe)PP)Ru(NO)R compounds at $E_1^{\circ\prime}$ = +0.77 (R = Me) and $E_1^{\circ\prime}$ = +0.74 V (R = Et) are significantly more negative than

dx.doi.org/10.1021/om200601g | *Organometallics* 2012, 31, 827−834

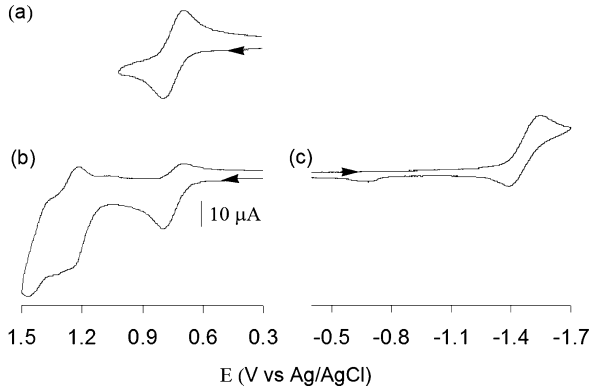

Figure 3. Cyclic voltammograms of 1 mM (T(*p*-OMe)PP)Ru(NO)Et in CH_2Cl_2 containing 0.1 M NBu_4PF_6 at a scan rate of 0.2 V/s at room temperature: (a) cyclic voltammogram showing only the first oxidation; (b) cyclic voltammogram scanned from +0.30 to +1.50 V; (c) cyclic voltammogram scanned from −0.40 to −1.70 V. Potentials are referenced to the Ag/AgCl couple.

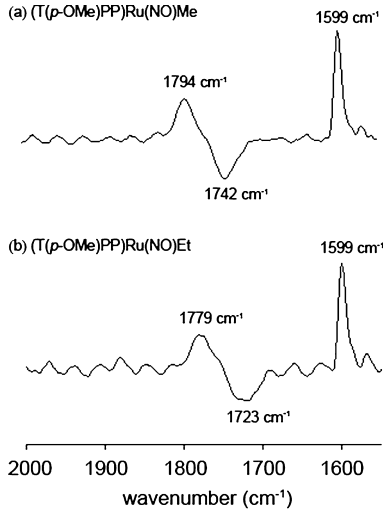

Figure 4. Difference IR spectra showing the products from the first oxidation of (a) (T(*p*-OMe)PP)Ru(NO)Me and (b) (T(*p*-OMe)PP)Ru(NO)Et in CH_2Cl_2 containing 0.1 M NBu_4PF_6, with the potentials held at 0.86 V vs Ag/AgCl.

that reported for the (T(*p*-OMe)PP)Ru(NO)Cl compound at $E_1^{\circ\prime}$ = +0.93 V,[27] consistent with the presence of the strongly electron donating alkyl ligands.

Further, the difference of 0.53 V in potentials between the first ($E_1^{\circ\prime}$) and second ($E_2^{\circ\prime}$) oxidations for (T(*p*-OMe)PP)Ru(NO)Me is larger than that for the (T(*p*-OMe)PP)Ru(NO)Cl compound ($E_2^{\circ\prime} - E_1^{\circ\prime}$ = 0.42 V); the difference is due primarily to the much lower first oxidation potential of the methyl derivative (both compounds have similar $E_2^{\circ\prime}$ values). We note that reversible first oxidations were also observed previously for the $[(por)Ru(NO)(H_2O)]^+$ cations (por = TPP,[30,31] TTP,[28] OEP[31]). However, and as noted in the Introduction, the oxidation of the six-coordinate (OEP)$RuPh_2$ compound is irreversible and involves a Ru-to-N_{por} migration of the Ph group;[17] in contrast, the first oxidation of the five-coordinate (OEP)Ru(THF)Ph compound does not lead to the migration of the Ph group.[17]

Infrared Spectroelectrochemistry. To investigate the site(s) of redox events in the six-coordinate (T(*p*-OMe)PP)Ru(NO)R (R = Me, Et) compounds, we performed fiber-optic infrared spectroelectrochemistry measurements of these compounds at room temperature while holding the electrode potential just beyond what was needed to achieve the first oxidation or reduction.

The difference IR spectra reveal the changes that occur (using the IR spectrum of the respective neutral (T(*p*-OMe)PP)Ru(NO)R compound as the background) in the spectra between 1550 and 2000 cm^{-1}. The difference IR spectrum for the first oxidation of (T(*p*-OMe)PP)Ru(NO)Me is shown in Figure 4a, and shows the consumption of the ν_{NO} band of the starting material at 1742 cm^{-1} and the formation of a new compound displaying a new ν_{NO} band at 1794 cm^{-1}. The relatively small shift in ν_{NO} ($\Delta\nu_{NO}$ = 52 cm^{-1}) is indicative of a porphyrin-centered first oxidation. The characteristic IR marker bands for oxidized tetraarylporphyrins (π cation radicals) are in the 1270−1295 cm^{-1} range.[46] Unfortunately, strong absorptions of the solvent system in this region do not allow for the identification of these marker bands. A new band at 1599 cm^{-1} was also observed in the difference IR spectrum (Figure 4a). In order to determine if this band was associated with the oxidized porphyrin macrocycle, IR spectroelectrochemical experiments using the non-nitrosyl H_2T(*p*-OMe)PP and (T(*p*-OMe)PP)Ru(CO) compounds were performed; similar new bands at ∼1600 cm^{-1} were observed upon the first oxidations of these compounds (data not shown). In addition, a 1600 cm^{-1} band in the IR spectrum of the (TPP)FeCl compound shifts to a band at 1584 cm^{-1} upon one-electron oxidation of the compound;[47] this shift was assigned to absorption changes of phenyl modes after the one-electron porphyrin-centered oxidation. Thus, combined with the relatively small shift in ν_{NO}, we conclude that the new band at 1599 cm^{-1} in Figure 4a is most likely due to the phenyl mode absorption changes of the porphyrin macrocycle upon the first oxidation.

The IR spectroelectrochemistry results for the first oxidation of (T(*p*-OMe)PP)Ru(NO)Et are similar to those for (T(*p*-OMe)PP)Ru(NO)Me (Figure 4b). The relatively small $\Delta\nu_{NO}$ value of 56 cm^{-1} is likewise attributed to a porphyrin-based first oxidation for (T(*p*-OMe)PP)Ru(NO)Et. We note that other Ru nitrosyl porphyrins such as (T(*p*-OMe)PP)Ru(NO)Cl[27] and (OEP)Ru(NO)(OEt)[29] also undergo porphyrin-based first oxidations.

The reductions of (T(*p*-OMe)PP)Ru(NO)Me and (T(*p*-OMe)PP)Ru(NO)Et were also examined by IR spectroelectrochemistry. As shown in Figure 5a, the reduction of (T(*p*-OMe)PP)Ru(NO)Me results in loss of the initial ν_{NO} band at 1742 cm^{-1}; however, no new ν_{NO} band was observed in the spectral window available to us. The reduction of (T(*p*-OMe)PP)Ru(NO)Et shows a similar disappearance of the initial ν_{NO} band at ∼1723 cm^{-1} (Figure 5b). We attribute the disappearance of the band at 1608 cm^{-1} to a change in porphyrin ring absorptions during the reduction process.

Kaim and co-workers[31] reported the electrochemical and spectroelectrochemical properties of the $[(por)Ru(NO)(L)]^+$ compounds (L = pyridine and substituted pyridines), and they showed that the reductions of these compounds shifted the ν_{NO} bands by ∼300 cm^{-1} to lower energy. Their DFT calculations supported their conclusions that the reductions were largely NO-centered. If such NO-centered reductions occurred for our (por)Ru(NO)R compounds, the expected new bands in the ∼1440 cm^{-1} region would fall outside our spectroelectrochemical spectral window. Due to the low chemical reversibility of the reductions for the (por)Ru(NO)R compounds at lower

dx.doi.org/10.1021/om200601g | *Organometallics* 2012, 31, 827−834

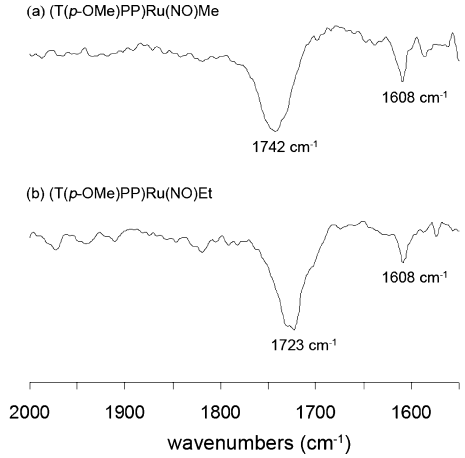

Figure 5. Difference IR spectra showing the results of the first reduction of (a) (T(*p*-OMe)PP)Ru(NO)Me and (b) (T(*p*-OMe)PP)Ru(NO)Et in CH_2Cl_2 containing 0.1 M NBu_4PF_6, with the potentials held at −1.65 and −1.63 V vs Ag/AgCl, respectively.

scan rates, it is more likely that eventual NO dissociation occurs from these electron-rich complexes under our spectroelectrochemical conditions. This is consistent with the presence of a long Ru−N(O) bond in the X-ray crystal structure of (T(*p*-OMe)PP)Ru(NO)Et that might be expected to favor NO dissociation.

In summary, we have prepared and determined the redox behavior of a representative set of (por)Ru(NO)R compounds that differ in tetraarylporphyrin and alkyl substitution. We show by fiber-optic infrared spectroelectrochemistry that the first oxidations of these compounds are porphyrin-based. In the neutral precursors, we demonstrate a trans influence of the NO ligand on the ^{1}H NMR spectroscopic shifts of the alkyl groups, an influence that results in a marked upfield shift of the proton signals for alkyl H atoms close to Ru. In addition, we have obtained the first X-ray crystal structure of an organometallic nitrosyl porphyrin containing an alkyl ligand. The structure reveals a cisoid arrangement of the trans ligands and a significant bending of the axial ligands away from the porphyrin normal.

EXPERIMENTAL SECTION

All reactions were performed under an atmosphere of prepurified nitrogen using standard Schlenk glassware and/or in an Innovative Technology Labmaster 100 Drybox. Solutions for spectral studies were also prepared under a nitrogen atmosphere. Solvents were distilled from appropriate drying agents under nitrogen just prior to use: CH_2Cl_2 (CaH_2), $CHCl_3$ (CaH_2), THF (CaH_2), hexane (CaH_2), benzene (Na), and toluene (Na).

Chemicals. The compounds (T(*p*-OMe)PP)Ru(NO)Cl and (T(*p*-CF_3)PP)Ru(NO)Cl ((T(*p*-OMe)PP) = tetrakis(*p*-methoxyphenyl)-porphyrinato dianion; (T(*p*-CF_3)PP) = tetra(*para*-trifluoromethylphenyl)porphyrinato dianion) were prepared from the reaction of the (por)Ru(NO)(O-*i*-C_5H_{11}) precursors with BCl_3 as described previously.[27] $AlMe_3$ (2.0 M in toluene), $AlEt_3$ (1.9 M in toluene), MeMgBr (1.0 M in toluene/THF (3/1)), and EtMgBr (1.0 M in THF) were purchased from Aldrich Chemical Co. and used as received. Ferrocene (Cp_2Fe; Cp = η^5-cyclopentadienyl anion, 98%) was purchased from Aldrich Chemical Co. and sublimed prior to use. NBu_4PF_6 (98%; Aldrich Chemical Co.) was recrystallized from hot ethanol. Chloroform-*d* (99.8%) was obtained from Cambridge Isotope Laboratories, purified by three freeze−pump−thaw cycles, and stored over Linde 4 Å molecular sieves. Elemental analyses were performed by Atlantic Microlab, Norcross, GA.

Instrumentation. Electrochemical measurements were performed using a BAS CV-50W instrument (Bioanalytical Systems, West Lafayette, IN) as described previously.[27,29] The solutions for all electrochemical experiments were deaerated by bubbling prepurified nitrogen through the solution for 10 min before each set of measurements, and then a nitrogen atmosphere was maintained during the measurements.

Infrared spectra for the synthetic work were performed on a Bio-Rad FT-155 FTIR spectrometer. For the spectroelectrochemical experiments, the infrared spectra were recorded using a Bruker Vector 22 FTIR spectrometer equipped with a mid-IR fiber-optic dip probe and liquid nitrogen cooled MCT detector (Remspec Corporation, Sturbridge, MA). Proton NMR spectra were obtained on a Varian 300 MHz spectrometer and the signals referenced to the residual signal of the solvent employed ($CDCl_3$ at 7.26 ppm). All coupling constants are in Hz.

Preparation of (T(*p*-X)PP)Ru(NO)R Compounds (X = OMe, CF_3; R = Me, Et). *Method I.* All compounds were synthesized at room temperature under reduced laboratory lighting. The following reaction is representative.

(T(p-OMe)PP)Ru(NO)Me. To a toluene solution (20 mL) of (T(*p*-OMe)PP)Ru(NO)Cl (0.050 g, 0.056 mmol) was added $AlMe_3$ (0.11 mL, 2.0 M in toluene, 0.22 mmol). The mixture was stirred under reduced lighting for 30 min, during which time the color changed from brownish green to dark green. The progress of the reaction was monitored by IR spectroscopy; however, we found that removal of the toluene solvent from the aliquots and redissolution of the product in CH_2Cl_2 gave more defined IR spectra. We also monitored the reactions by thin-layer chromatography using a 1/1 benzene/hexane mixture. After the reaction was complete, the solvent was removed in vacuo, the residue was dissolved in benzene (10 mL), and the solution was transferred to the top of a neutral alumina column (1 × 15 cm) prepared in hexane. Elution with a benzene/hexane (1/1) mixture under nitrogen yielded a green band. The green band was collected and taken to dryness in vacuo. The residue was dissolved in $CHCl_3$/hexane (5 mL, 4/1), and slow evaporation of the solvent mixture under an inert atmosphere gave microcrystals of the product (0.023 g, 47% isolated yield). IR (CH_2Cl_2, cm^{-1}): ν_{NO} 1742. IR (KBr, cm^{-1}): ν_{NO} 1735; also 1606 m, 1528 m, 1510 m, 1286 m, 1243 s, 1174 s, 1070 w, 1015 s, 849 w, 809 m, 715 w, 609 w. ^{1}H NMR ($CDCl_3$, ppm): δ 8.89 (s, 8H, pyrrole-H of T(*p*-OMe)PP), 8.20 (d, 4H, J = 7 Hz, *o*-H of T(*p*-OMe)PP, 8.11 (d, 4H, J = 7 Hz, *o*′-H of T(*p*-OMe)PP), 7.30 (t, 8H, J = 6 Hz, *m*-H of T(*p*-OMe)PP), 4.11 (s, 12H, OCH_3 of T(*p*-OMe)PP), −6.72 (s, 3H, CH_3).

(T(p-CF3)PP)Ru(NO)Me. The (T(*p*-CF_3)PP)Ru(NO)Me compound was generated similarly (using 2-fold excess $Al(Me)_3$) in 28% isolated yield. Anal. Calcd for $C_{49}H_{27}F_{12}N_5ORu{\cdot}0.03CHCl_3$: C, 56.93; H, 2.63; N, 6.77; Cl, 0.31. Found: C, 56.55; H, 2.98; N, 6.32; Cl, 0.28. IR (CH_2Cl_2, cm^{-1}): ν_{NO} 1748. IR (KBr, cm^{-1}): ν_{NO} 1735; also 1616 m, 1404 m, 1324 s, 1168 m, 1129 s, 1068 m, 1013 s, 814 m, 797 m, 717 w. ^{1}H NMR ($CDCl_3$, ppm): δ 8.82 (s, 8H, pyrrole-H of T(*p*-CF_3)PP), 8.41 (d, 4H, J = 7 Hz, *o*-H of T(*p*-CF_3)PP), 8.33 (d, 4H, J = 7 Hz, *o*′-H of T(*p*-CF_3)PP), 8.06 (app t (overlapping d's), 8H, J = 6, *m*/*m*′-H of T(*p*-CF_3)PP), −6.71 (s, 3H, CH_3).

(T(p-OMe)PP)Ru(NO)Et. The (T(*p*-OMe)PP)Ru(NO)Et compound was generated similarly (using 2-fold excess $Al(Et)_3$) in 56% isolated yield. Anal. Calcd for $C_{50}H_{41}N_5O_5Ru{\cdot}0.1CHCl_3$: C, 66.50; H, 4.58; N, 7.74; Cl, 1.18. Found: C, 66.34; H, 4.53; N, 7.74; Cl, 1.18. IR (CH_2Cl_2, cm^{-1}): ν_{NO} 1723. IR (KBr, cm^{-1}): ν_{NO} 1724; also 1606 m, 1527 w, 1510 m, 1349 m, 1245 s, 1174 s, 1070 w, 1015 s, 849 w, 808 m, 715 w, 609 w. ^{1}H NMR ($CDCl_3$, ppm): δ 8.87 (s, 8H, pyrrole-H of T(*p*-OMe)PP), 8.19 (d, 4H, J = 7 Hz, *o*-H of T(*p*-OMe)PP), 8.10 (d, 4H, J = 7 Hz, *o*′-H of T(*p*-OMe)PP), 7.29 (t, 8H, *m*-H of T(*p*-OMe)PP), 4.11 (s, 12H, OCH_3 of T(*p*-OMe)PP), −4.19 (t, 3H, J = 8, CH_2CH_3), −6.00 (q, 2H, J = 8, CH_2CH_3).

A suitable dark green prism-shaped crystal was grown by slow evaporation of a CH_2Cl_2/hexane/benzene (2/1/trace) solution of (T(*p*-OMe)PP)Ru(NO)Et at room temperature under an inert atmosphere.

Method II. The following reaction is representative of the reactions at room temperature.

(T(p-OMe)PP)Ru(NO)Me. To a THF solution (20 mL) of (T(*p*-OMe)PP)Ru(NO)Cl (0.080 g, 0.090 mmol) was added MeMgBr (0.16 mL, 1.4 M in toluene/THF (3/1), 0.22 mmol). The mixture was stirred under reduced lighting for 1 h, and all solvent was removed in vacuo. The resulting solid was dissolved in a minimum amount of benzene (7 mL) and filtered through a neutral alumina column (1 × 15 cm) with benzene as eluent. The green fraction was collected and taken to dryness in vacuo. The residue was dissolved in a $CHCl_3$/hexane (5 mL, 4/1), and slow evaporation of the solvent mixture under an inert atmosphere gave (T(*p*-OMe)PP)Ru(NO)Me (0.018 g, 0.020 mmol, 23% isolated yield).

(T(p-CF$_3$)PP)Ru(NO)Me. The (T(*p*-CF_3)PP)Ru(NO)Me compound was generated similarly (2-fold excess using MeMgBr, 5 h reaction time) in 18% isolated yield.

(T(p-CF$_3$)PP)Ru(Me)$_2$. The (T(*p*-CF_3)PP)Ru$(Me)_2$ compound was generated similarly (using 9-fold excess MeMgBr, 1 h reaction time). ^{1}H NMR ($CDCl_3$, ppm): δ 8.25 (s, 8H, pyrrole-H of T(*p*-CF_3)PP), 8.19 (d, 8H, J = 8.4 Hz, *o*-H of T(*p*-CF_3)PP), 7.98 (d, 8H, J = 8 Hz, *m*-H of T(*p*-CF_3)PP), −2.71 (s, 6H, CH_3).

(T(p-OMe)PP)Ru(NO)Et. The (T(*p*-OMe)PP)Ru(NO)Et compound was generated similarly (using EtMgBr, 1.0 M in THF, 2-fold excess, 80 min reaction time) in 26% isolated yield.

(T(p-CF$_3$)PP)Ru(NO)Et. The (T(*p*-CF_3)PP)Ru(NO)Et compound was generated similarly (using EtMgBr, 1.0 M in THF, 2-fold excess, 1 h reaction time) in 17% isolated yield. IR (CH_2Cl_2, cm^{-1}): ν_{NO} 1735. IR (KBr, cm^{-1}): ν_{NO} 1735; also 1617 m, 1405 m, 1324 s, 1169 s, 1128 s, 1069 s, 1013 s, 858 m, 814 m, 716 w, 684 w. ^{1}H NMR ($CDCl_3$, ppm): δ 8.81 (s, 8H, pyrrole-H of T(*p*-CF_3)PP), 8.42 (d, 4H, J = 8 Hz, *o*-H of T(*p*-CF_3)PP), 8.33 (d, 4H, J = 8 Hz, *o′*-H of T(*p*-CF_3)PP), 8.06 (app t (overlapping d's), 8H, J = 7, *m*/*m′*-H of T(*p*-CF_3)PP), −4.17 (t, 3H, J = 8, CH_2CH_3), −5.96 (q, 2H, J = 8, CH_2CH_3).

Solid-State Structural Determination of (T(*p*-OMe)PP)Ru(NO)Et. Details of the crystal data and refinement are given in Table 6.

Table 6. Crystal Data and Structure Refinement

compd	(T(*p*-OMe)PP)Ru(NO)Et[a]
formula (fw)	$C_{50}H_{41}N_5O_5Ru{\cdot}CH_2Cl_2$ (977.87)
T (K)	103(2)
cryst syst	monoclinic
space group	$P2_1/n$
a (Å), α (deg)	14.5153(15), 90
b (Å), β (deg)	18.666(2), 95.930(2)
c (Å), γ (deg)	15.9805(17), 90
V (Å^3), Z/Z'	4306.6(8), 4/1
D(calcd), g/cm^3	1.508
abs coeff, mm^{-1}	0.545
F(000)	2008
cryst size (mm)	0.36 × 0.14 × 0.12
θ range for data collecn (deg)	1.68−27.53
no. of rflns collected	51 341
no. of indep rflns	9874 (R_{int} = 0.0508)
max and min transmission	0.9375 and 0.8279
no. of data/restraints/params	9874/16/605
goodness of fit on F^2	1.056
final R1 ($I > 2\sigma(I)$)	0.0442
wR2 (all data)	0.1217
largest diff peak and hole (e Å^{-3})	1.311 and −0.717

[a]This compound crystallizes as a dichloromethane solvate.

Single-crystal X-ray diffraction data of a suitable red prism-shaped crystal were collected using a Bruker APEX CCD area detector with graphite-monochromated Mo Kα radiation (λ = 0.710 73 Å).

Cell parameters were determined from a nonlinear least-squares fit of 9782 peaks in the range 3.2 < θ < 26.4°. A total of 51 341 data were measured in the range 1.68 < θ < 27.53° using ω oscillation frames. The data were corrected for absorption by the semiempirical from equivalents method. The data were merged to form a set of 9874 independent data with R(int) = 0.0508 and a coverage of 100.0%. The monoclinic space group $P2_1/n$ was determined by systematic absences and statistical tests and verified by subsequent refinement. The structure was solved by direct methods and using the SHELXTL system and refined by full-matrix least-squares methods on F^2. The axial ligands, NO and ethyl, and hence the metal were disordered and modeled in two orientations. The occupancies of the disordered atoms refined to 0.554(15) and 0.446(15) for the unprimed and primed atoms, respectively. Restraints on the positional and displacement parameters of the disordered atoms were required. Also, the atoms in the axial groups directly bonded to the metals were constrained to have the same displacement parameters. Non-hydrogen atoms were refined with anisotropic displacement parameters. Hydrogen atom displacement parameters were set to 1.2× (1.5× for methyl) the isotropic equivalent displacement parameters of the bonded atoms. A total of 605 parameters were refined against 16 restraints and 9874 data to give wR2(F^2) = 0.1178 and S = 1.056 for weights of $w = 1/[\sigma^2(F^2) + (0.0640P)^2 + 4.4000P]$, where $P = [F_o^2 + 2F_c^2]/3$. The final R1(F) value was 0.0442 for the 9145 observed ($F > 4\sigma(F)$) data. The largest shift/su was 0.001 in the final refinement cycle. Thermal ellipsoids for Figure 1 are drawn at the 35% probability level. CCDC 862081 contains the supplementary crystallographic data for this paper. These data can be obtained free of charge from The Cambridge Crystallographic Data Centre via www.ccdc.cam.ac.uk/data_request/cif.

■ ASSOCIATED CONTENT

Ⓢ Supporting Information

A CIF file giving crystallographic data for (T(*p*-OMe)PP)Ru(NO)Et. This material is available free of charge via the Internet at http://pubs.acs.org.

■ AUTHOR INFORMATION

Corresponding Author

*Tel: (405) 325-6401. E-mail: xunan@ou.edu (N.X.); grichteraddo@ou.edu (G.B.R.-A.).

■ ACKNOWLEDGMENTS

We are grateful to the National Science Foundation (CHE-0911537 to G.B.R.-A.) for funding for this work. We thank Professor Brian R. James (Canada) for very helpful discussions regarding ruthenium porphyrin chemistry, Dr. Li Chen for assistance with some of the earlier synthetic work and for helpful discussions, and Dr. Masood Khan for assistance with the X-ray diffraction data collection.

■ REFERENCES

(1) Brothers, P. J. *Adv. Organomet. Chem.* **2001**, *46*, 223−321.
(2) Brothers, P. J.; Collman, J. P. *Acc. Chem. Res.* **1986**, *19*, 209−215.
(3) Setsune, J.-I.; Dolphin, D. *Can. J. Chem.* **1987**, *65*, 459−467.
(4) Mansuy, D. *Pure Appl. Chem.* **1987**, *59*, 759−770.
(5) Augusto, O.; Kunze, K. L.; Demontellano, P. R. O. *J. Biol. Chem.* **1982**, *257*, 6231−6241.
(6) Ortiz de Montellano, P. R.; Kerr, D. E. *Biochemistry* **1985**, *24*, 1147−1152.
(7) Lagrange, G.; Cocolios, P.; Guilard, R. *J. Organomet. Chem.* **1984**, *260*, C16−C20.
(8) Lançon, D.; Cocolios, P.; Guilard, R.; Kadish, K. M. *J. Am. Chem. Soc.* **1984**, *106*, 4472−4478.
(9) Lançon, D.; Cocolios, P.; Guilard, R.; Kadish, K. M. *Organometallics* **1984**, *3*, 1164−1170.
(10) Kadish, K. M.; Lançon, D.; Cocolios, P.; Guilard, R. *Inorg. Chem.* **1984**, *23*, 2372−2373.

(11) Guilard, R.; Boisselier-Cocolios, B.; Tabard, A.; Cocolios, P.; Simonet, B.; Kadish, K. M. *Inorg. Chem.* **1985**, *24*, 2509−2520.
(12) Guilard, R.; Lagrange, G.; Tabard, A.; Lançon, D.; Kadish, K. M. *Inorg. Chem.* **1985**, *24*, 3649−3656.
(13) Cheng, L.; Richter-Addo, G. B. In *The Porphyrin Handbook*; Guilard, R., Smith, K., Kadish, K. M., Eds.; Academic Press: New York, 2000; Vol. *4* (Biochemistry and Binding: Activation of Small Molecules), pp 219−291.
(14) Seyler, J. W.; Fanwick, P. E.; Leidner, C. R. *Inorg. Chem.* **1990**, *29*, 2021−2023.
(15) Seyler, J. W.; Fanwick, P. E.; Leidner, C. R. *Inorg. Chem.* **1992**, *31*, 3699−3700.
(16) Seyler, J. W.; Leidner, C. R. *J. Chem. Soc., Chem. Commun.* **1989**, 1794−1796.
(17) Seyler, J. W.; Leidner, C. R. *Inorg. Chem.* **1990**, *29*, 3636−3641.
(18) Seyler, J. W.; Safford, L. K.; Fanwick, P. E.; Leidner, C. R. *Inorg. Chem.* **1992**, *31*, 1545−1547.
(19) Alexander, C. S.; Rettig, S. J.; James, B. R. *Organometallics* **1994**, *13*, 2542−2544.
(20) Collman, J. P.; Ha, Y.; Wagenknecht, P. S.; Lopez, M.-A.; Guilard, R. *J. Am. Chem. Soc.* **1993**, *115*, 9080−9088.
(21) Ke, M.; Rettig, S. J.; James, B. R.; Dolphin, D. *J. Chem. Soc., Chem. Commun.* **1987**, 1110−1112.
(22) Ke, M.; Sishta, C.; James, B. R.; Dolphin, D.; Sparapany, J. W.; Ibers, J. A. *Inorg. Chem.* **1991**, *30*, 4766−4771.
(23) Sishta, C.; Ke, M.; James, B. R.; Dolphin, D. *J. Chem. Soc., Chem. Commun.* **1986**, 787−788.
(24) Collman, J. P.; Brothers, P. J.; McElwee-White, L.; Rose, E. *J. Am. Chem. Soc.* **1985**, *107*, 6110−6111.
(25) Collman, J. P.; Rose, E.; Venburg, G. D. *J. Chem. Soc., Chem. Commun.* **1994**, 11−12.
(26) Guilard, R.; Kadish, K. M. *Chem. Rev.* **1988**, *88*, 1121−1146.
(27) Xu, N.; Lee, J.; Powell, D. R.; Richter-Addo, G. B. *Inorg. Chim. Acta* **2005**, *358*, 2855−2860.
(28) Bohle, D. S.; Hung, C.-H.; Smith, B. D. *Inorg. Chem.* **1998**, *37*, 5798−5806.
(29) Carter, S. M.; Lee, J.; Hixson, C. A.; Powell, D. R.; Wheeler, R. A.; Shaw, M. J.; Richter-Addo, G. B. *Dalton Trans.* **2006**, 1338−1346.
(30) Kadish, K. M.; Adamian, V. A.; Caemelbecke, E. V.; Tan, Z.; Tagliatesta, P.; Bianco, P.; Boschi, T.; Yi, G.-B.; Khan, M. A.; Richter-Addo, G. B. *Inorg. Chem.* **1996**, *35*, 1343−1348.
(31) Singh, P.; Das, A. K.; Sarkar, B.; Niemeyer, M.; Roncaroli, F.; Olabe, J. A.; Fiedler, J.; Zalis, S.; Kaim, W. *Inorg. Chem.* **2008**, *47*, 7106−7113.
(32) Richter-Addo, G. B.; Wheeler, R. A.; Hixon, C. A.; Chen, L.; Khan, M. A.; Ellison, M. K.; Schulz, C. E.; Scheidt, W. R. *J. Am. Chem. Soc.* **2001**, *123*, 6314−6326.
(33) Hodge, S. J.; Wang, L.-S.; Khan, M. A.; Young, V. G. Jr.; Richter-Addo, G. B. *Chem. Commun.* **1996**, 2283−2284.
(34) Cheng, L.; Chen, L.; Chung, H.-S.; Khan, M. A.; Richter-Addo, G. B.; Young, V. G. Jr. *Organometallics* **1998**, *17*, 3853−3864.
(35) Ghosh, A. *Acc. Chem. Res.* **2005**, *38*, 943−954.
(36) Ghosh, A.; Bocian, D. F. *J. Phys. Chem.* **1996**, *100*, 6363−6367.
(37) Wyllie, G. R. A.; Scheidt, W. R. *Chem. Rev.* **2002**, *102*, 1067−1089.
(38) Leung, W.-H.; Hun, T. S. M.; Wong, K.-Y.; Wong, W.-T. *J. Chem. Soc., Dalton Trans.* **1994**, 2713−2718.
(39) Yang, S.-Y.; Leung, W.-H.; Lin, Z. *Organometallics* **2001**, *20*, 3198−3201.
(40) Hansen, T.; Ovesen, H.; Svadberg, A.; Svendsen, K.; Tangen, E.; Swarts, J. C.; Ghosh, A. *Organometallics* **2004**, *23*, 3870−3872.
(41) Ke, M. Ph.D. Thesis, Department of Chemistry, The University of British Columbia, 1988.
(42) Alenxander, C. S. Ph.D. Thesis, Department of Chemistry, The University of British Columbia, Canada, 1995.
(43) Galardon, E.; Le Maux, P.; Toupet, L.; Simonneaux, G. *Organometallics* **1998**, *17*, 565−569.
(44) Harada, T.; Wada, S.; Yuge, H.; Miyamoto, T. K. *Acta Crystallogr., Sect. C* **2003**, *59*, M37−M39.
(45) Kawai, M.; Yuge, H.; Miyamoto, T. K. *Acta Crystallogr., Sect. C* **2002**, *58*, M581−M582.
(46) Shimomura, E. T.; Phillippi, M. A.; Goff, H. M.; Scholz, W. F.; Reed, C. A. *J. Am. Chem. Soc.* **1981**, *103*, 6778−6780.
(47) Jones, D. H.; Hinman, A. S. *J. Chem. Soc., Dalton Trans.* **1992**, 1503−1508.